ACS APPLIED MATERIALS & INTERFACES

Research Article

www.acsami.org

Superhydrophobic Surfaces from Hierarchically Structured Wrinkled Polymers

Yinyong Li,[†] Shuxi Dai,[‡] Jacob John,[†] and Kenneth R. Carter*,[†]

[†]Department of Polymer Science and Engineering, University of Massachusetts, 120 Governors Drive, Amherst, Massachusetts 01003-9263, United States

[‡]Key Laboratory for Special Functional Materials of Ministry of Education, Henan University, Kaifeng 475004, P. R. China

ABSTRACT: This work reports the creation of superhydrophobic wrinkled surfaces with hierarchical structures at both the nanoscale and microscale. A nanoscale structure with 500 nm line gratings was first fabricated on poly(hydroxyethyl methacrylate) films by nanoimprint lithography while a secondary micro-scale structure was created by spontaneous wrinkling. Compared with random wrinkles whose patterns show no specific orientation, the hierarchical wrinkles exhibit interesting orientation due to confinement effects of pre-imprinted line patterns. The hierarchically wrinkled surfaces have significantly higher water contact angles than random wrinkled surfaces, exhibiting superhydrophobicity with water contact angles higher than 160° and water sliding angle lower than 5°. The hierarchically structured wrinkled surfaces exhibit tunable wettability from hydrophobic to superhydrophobic and there is an observed transition from anisotropic to isotropic wetting behavior achievable by adjusting the initial film thickness.

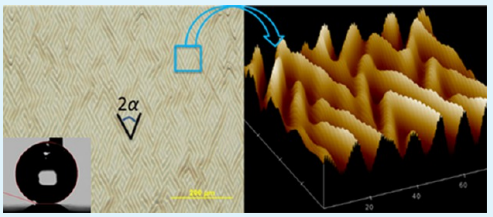

KEYWORDS: *wrinkling, hierarchical structures, polymer, nanoimprint lithography, superhydrophobic, anisotropic wetting*

INTRODUCTION

Dating back to pioneer research work in the early 20th century, superhydrophobic surfaces have been extensively studied in recent years.[1] Typically defined as a surface with a water contact angle (CA) greater than 150° and contact angle hysteresis (CAH) of less than 10°, superhydrophobic surface research is often inspired by natural examples, such as the self-cleaning effect of the lotus leaf and water repellency of some insects, the superhydrophobic effect has found numerous applications in the areas of antibiofouling, antisticking, self-cleaning, drag-reduction, etc.[2−4] In principle, artificial superhydrophobic surfaces can be produced through the combination of controlled surface roughness with low-surface-energy coatings.[5] It has been suggested that hierarchical structures with hierarchically structured roughness on both the nanoscale and microscale could help to improve superhydrophobicity.[3,6] Numerous methods for developing superhydrophobic structures have been reviewed, including layer-by-layer assembly, imprinting, electrospinning, hydrothermal treatment, plasma etching, etc.[1,7,8] Imprint lithography, with its simplicity, high precision, high fidelity, and low cost, lends itself to facile fabrication of numerous structures ranging from nanoscale to microscale.[9,10] Zhang et al. reported anisotropic wettability on hierarchical structures prepared by sequential imprinting.[11] Liu et al. prepared superhydrophobic polymer films via transfer-printing lithography with an aluminum oxide mold.[12] Plant leaf,[13,14] butterfly wing,[15] and gecko foot hairs[16] structures have been replicated by imprint lithography using either molds of natural materials or artificially fabricated biomimetic patterns.

Alternatively, recent developments in spontaneous surface wrinkling[17−19] provide a simple but efficient way to create either microscale or nanoscale textured structures. There have been several attempts to fabricate hierarchically wrinkled surfaces with specific wetting properties by combining spontaneous wrinkling with other techniques, such as imprint lithography and plasma treatment. Zhang et al.[20] discussed the theoretical possibility of multiscale hierarchical wrinkles induced by mechanical strain on multilayer films, which can be switched between superhydrophobic and superhydrophilic simply by strain control. Several studies have successfully manufactured superhydrophobic hierarchical structures consisting of wrinkle patterns with micropillars,[21] nanopillars,[22] silica nanoparticles[23] as well as silver nanoflakes.[24] More interestingly, by controlling hierarchically wrinkled structures, biomimetic surfaces can be prepared with special wetting behavior. For example, Lee and coauthors reported biomimetic rice-leaf surfaces showing anisotropic wetting and superhydrophobicity.[6]

We have recently reported the development a simple and general method for the preparation of functional wrinkled poly(hydroxyethylmethacrylate) (PHEMA) films via a reactive methyltrichlorosilane infusion reaction.[25] Patterned polymer films with wrinkled surface structures and tailored surface chemistry were obtained using this facile chemically induced wrinkling process. The height and periodicity of wrinkles were controlled from the nanoscale to microscale by simply adjusting the original film thickness. A typical wrinkled PHEMA film showed enhanced hydrophobic behavior with a water contact

Received: August 8, 2013
Accepted: October 16, 2013
Published: October 16, 2013

angle of about 100° compared with the control hydrophilic flat PHEMA film (CA = 34°).

Herein, we demonstrate a fabrication method that combines top-down nanoimprint lithography (NIL) with a bottom-up chemically induced wrinkling process for the fabrication of hierarchically wrinkled polymer films where we achieve complex surface structures with tunable wetting properties. In short we first prepare 500 nm period grating structures on flat PHEMA films by NIL. Hierarchical wrinkled structures containing the nanoscale grating patterns were then prepared using a silane infusion-induced wrinkling process.[25] The morphology and size of the surface structures is easily controlled by adjusting the initial thickness of the PHEMA film. The fabricated hierarchical structures exhibit tunable wettability from hydrophobic to superhydrophobic and display a transition from anisotropic to isotropic wetting behavior. This work presents a fresh perspective on this new material set that can be exploited to create hierarchically structured surfaces.

EXPERIMENTAL SECTION

Materials. All reagents were used as received without further purification unless otherwise specified. Methyltrichlorosilane was purchased from TCI America and 2-hydroxymethyl methacrylate was from Sigma-Aldrich (7−8% vinylmethylsiloxane)-(dimethylsiloxane) copolymer and (25−30% methylhydrosiloxane)-(dimethylsiloxane) copolymer were purchased from Gelest Inc. Dimethylformamide (DMF), ethanol and toluene (ACS reagent grade) were purchased from Fisher Scientific. Silicon wafers (orientation 100, thickness 605−645 μm) were purchased from University Wafer. Polydimethylsiloxane (PDMS) elastomer kits (Sylgard 184) were purchased from Dow Corning.

Fabrication of Prepatterned Nanostructures. Synthesis of poly(2-hydroxyethyl methacrylate) (PHEMA) by free radical polymerization is described in details previously.[25] A PHEMA/DMF solution was spin-coated at different speeds on clean silicon wafers to obtain flat films with different thicknesses. The PHEMA films were prebaked at 100 °C for 1 h to remove residual solvent before imprinting. A silicon master mold with 500 nm grating patterns, 1 μm pitch size, and aspect ratio (height to width of the lines) of 1 was used as master mold. A "hardened", cross-linked polydimethylsiloxane elastomer (h-PDMS) mold was obtained by replica molding of the silicon master mold according to the method described previously.[25,26] Flat PHEMA films were then imprinted with the h-PDMS mold at 120 °C with pressure of 300 psi for 2 min using a Nanonex NX-2000 nanoimprinter.

Fabrication of Hierarchically Wrinkled Pattern. PHEMA films with grating patterns were immersed in a solution of toluene containing methyltrichlorosilane (V/V: 100/5) solution and allowed to react at 100 °C for 2 h. Because of swelling and cross-linking of the film in the solution, microscale wrinkling was generated on the PHEMA films containing the lines pattern, giving rise to the formation of hierarchical structures. After the chemical wrinkling reaction, the PHEMA films were rinsed with toluene to remove any unreacted silane and dried with dry nitrogen gas. For comparison, flat PHEMA films without the nanoimprinted prepatterns were also wrinkled using the same method.

Characterization. Film thicknesses were measured using a Veeco Dektak Stylus Profilometer. Atomic Force Microscopy (AFM) images were collected on a Digital Instruments Nanoscope III in tapping mode under ambient conditions using silicon cantilevers (spring constant 0.58 N/m). Water contact angles and sliding angles were measured using a VCA Optima surface analysis/goniometry system with water droplets size of 5 μL. Both static and dynamic (advancing and receding) contact angles were recorded. Films surface structures were studied using an Olympus optical microscope.

RESULTS AND DISCUSSION

Figure 1 contains the schematic illustration of the process for fabricating (a) random wrinkles and (b) hierarchical wrinkled/

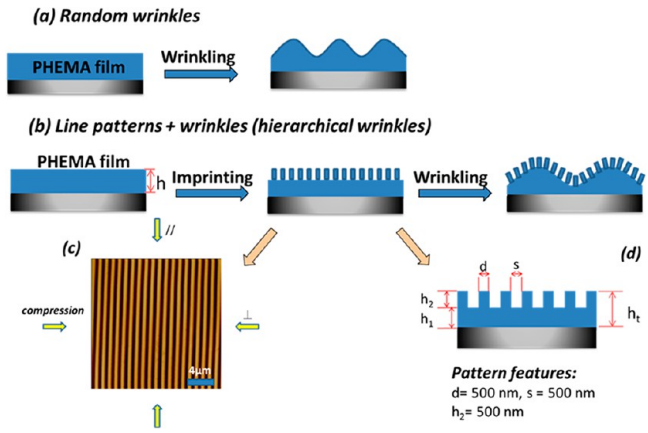

Figure 1. Schematic illustration of the process for generating random wrinkles and hierarchical wrinkle/line patterns on PHEMA films. (a) Random wrinkles via a reactive silane infusion-induced wrinkling method, (b) hierarchical wrinkle/line patterns fabricated by spontaneous wrinkling of pre-patterned PHEMA films, (c) top-view AFM image of the nanoimprinted prepattern and compression direction relative to pattern orientation, (d) schematic of cross-section of grating pattern.

patterned structures on the PHEMA films. The preparation of random microscale wrinkles was performed by silane infusion induced wrinkling as shown in Figure 1a. The mechanism of methyltrichlorosilane infusion and wrinkling by the resulting gradient of cross-linking within the polymer films has been described previously.[25] To obtain hierarchically ordered wrinkled structures, we prepatterned the PHEMA films with 500 nm period grating structures via NIL prior to the wrinkling process (Figure 1b). An AFM image of the features of the imprinted pattern is shown in Figure 1c and a schematic drawing in Figure 1d. After NIL patterning, hierarchical ordered wrinkles were generated on the pre-patterned PHEMA films via the silane infusion wrinkling process.

Figure 2 contains optical microscope and topographic AFM images of typical PHEMA films with random wrinkles (left) and hierarchical wrinkles (right) with prepatterned line gratings. Both sets of wrinkled films were prepared from initially flat PHEMA films with thickness of 3.4 μm. The optical observation in Figure 2a shows that the disordered wrinkles with a labyrinth pattern appear across the film surface. The image with a disc-shaped structure obtained from two-dimensional fast Fourier transform (FFT) analysis reveals that the generated wrinkle pattern is random and displays no specific directional orientation.[27]

Because of the isotropic swelling strain, the spontaneously generated wrinkle patterns are usually disordered. The presence of patterned nanostructures on surfaces to be wrinkled has been shown to be an effective route for the fabrication of hierarchical patterned surface in both theoretical and experimental studies.[28,29] Our hierarchical micro/nano wrinkled structures were created by inducing micro-size wrinkles on the PHEMA films imprinted with prepatterned line structures. As shown in the microscope image in Figure 2c, regularly ordered wrinkle structures with a herringbone-like pattern were obtained. The FFT image analysis of the resulting hierarchically wrinkled

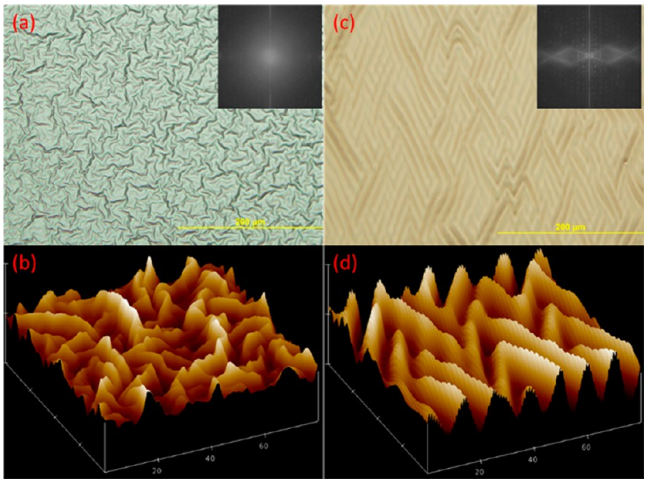

Figure 2. Optical microscope images and AFM images of (a, b) random wrinkles and (c, d) hierarchical wrinkles with prepatterned grooved nanostructures. The inset images are the corresponding fast Fourier transform image analysis.

surface (inset of Figure 2c) displays an interesting rhombus-shape pattern, which corresponds to the orientation of wrinkles observed on the surface of pre-patterned film. The AFM image in Figure 2d clearly showed the pre-patterned nanoscale grooved lines were preserved after the wrinkling process and these patterns are distributed uniformly over the surface of the microscale wrinkles.

A close observation of the surface by AFM reveals that the dimension and periodicity of imprinted grating nanostructures remained almost constant before and after chemically induced wrinkling (Figure 3). The as-imprinted PHEMA lines have a

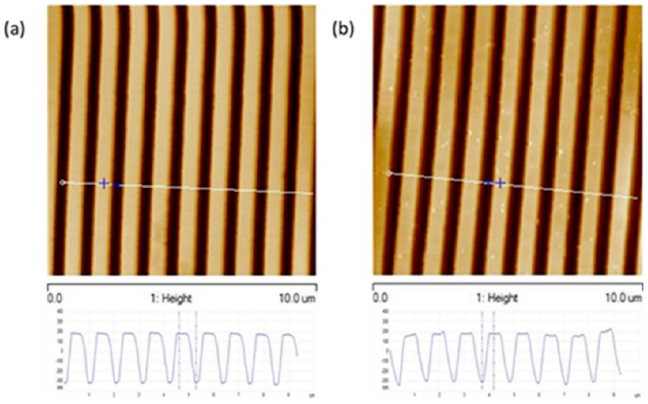

Figure 3. AFM images of imprinted grating nanostructures on the PHEMA films (a) before and (b) after wrinkling.

width and height of ~500 nm (Figure 3a), matching the size and depth of the *h*-PDMS mold grooves. After the silane infusion reaction and subsequent wrinkling, the AFM scan (Figure 3b) of the patterned lines reveals a width of 500 nm with sharp corners, consistent with the original imprinted grating structures. The line profile of the wrinkled grating structures shows the heights ranging from 470 to 495 nm, which is slightly reduced but still comparable to the initial height (500 nm) of grating structures on the imprinted PHEMA film.

The excellent control of wrinkle orientation and shape is due to geometric confinement by the grating patterns. While there have been reports on the control of wrinkle patterns with prepatterned structures, most of these studies concentrate on the effect of the pattern with much larger size scale than the size of wrinkles.[30−35] Only a few studies concerned the influence of pre-patterns on the formation of wrinkles with a similar or larger size scale as those of the patterns. For example, Ohzono et al.[36] reported the directional order of microwrinkles resulting from the spatial confinement of lithographic hexagonal microsphere patterns. Lee et al.[29] showed that grating patterns introduced to a surface on the nanoscale induce anisotropic mechanical properties to polymer films and play a significant role on determining the wavelength of subsequent mircoscale wrinkles. Here, we found a similar phenomenon that the incorporation of nanopatterns brings about interesting herringbone-like wrinkling topography to PHEMA film, which could be attributed to the anisotropic mechanical properties caused by grating patterns. In the case of surface instabilities, bending stiffness of the film plays a key role in wrinkle development. Due to the unidirectional line patterns, the bending stiffness in compression depends on the direction of strain relative to those line patterns. To analyze the ordering of wrinkles, we utilize a composite model proposed by Lee et al.[29] for patterned films to calculate the effective bending stiffness of film in different compression directions. Using the composite model, the effective bending stiffness for parallel ($D_{\parallel}$) and perpendicular ($D_{\perp}$) compression (Figure 1c) is expressed as

$$D_{\parallel} = \frac{Eh_t^3}{12}\varphi + \frac{Eh_1^3}{12}(1-\varphi) \quad (1)$$

$$D_{\perp} = \left[\frac{12}{Eh_t^3}\varphi + \frac{12}{Eh_1^3}(1-\varphi)\right]^{-1} \quad (2)$$

where h_t and h_1 are the maximum thickness and minimum thickness of the patterned film respectively, E is modulus of the film and φ is the fraction of surface area occupied by lines ($\varphi = d/(d+s)$) (Figure 1d). Herein, because the line width is 500 nm and pitch size is 1 μm, φ is equal to 0.5, and the expression of bending stiffness can be simplified as

$$D_{\parallel} = \frac{Eh_t^3}{24} + \frac{Eh_1^3}{24} \quad (3)$$

$$D_{\perp} = \left[\frac{6}{Eh_t^3} + \frac{6}{Eh_1^3}\right]^{-1} \quad (4)$$

The critical buckling stress, P_c, of a thin film is proportional to bending stiffness. For cases where $D_{\perp} < D_{\parallel}$, then $P_{c\perp} < P_{c\parallel}$, so the film tends to buckle first in the perpendicular direction when compression stress is higher than $P_{c\perp}$. The continuous building up of compression eventually leads to the buckling of the film in the parallel direction. The integrated effect of buckling in both directions builds up the final herringbone-like morphology of the wrinkles, similar to the herringbone winkle developed by sequential release of prestrain.[37,38]

From eq 3 and 4, the effective bending stiffness is related to total film thickness as well as the pre-pattern height. Therefore, the initial film thickness and pattern height will influence the final wrinkling morphology. To investigate this, a series of imprinted PHEMA films with varying initial thickness were fabricated with the same NIL patterns, i.e., changing h_1 while keeping h_2 constant, and these sample were subsequently

infused and wrinkled. The Optical microscopic images of hierarchical patterned/wrinkled PHEMA films with different initial thickness are shown in Figure 4. Most of the hierarchical

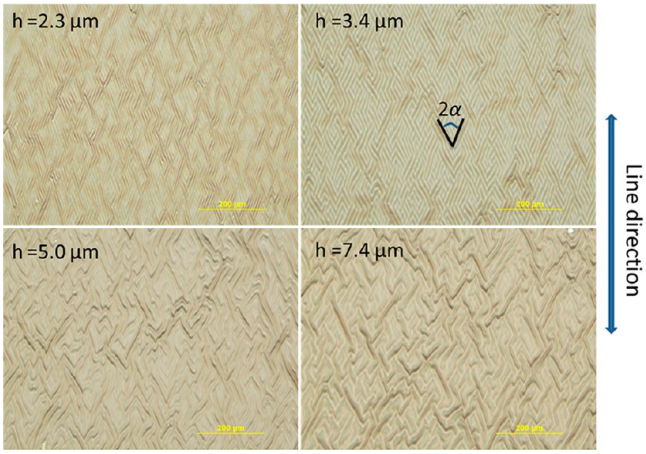

Figure 4. Optical microscopic images of hierarchical wrinkles with various film thicknesses.

films show relatively ordered wrinkle structures with a herringbone-like pattern. To better investigate the property of this wrinkle orientation phenomenon, the characteristic wrinkle angle, (2α), is defined as the angle between two strands of wrinkles. Figure 5 presents the relationship between α and

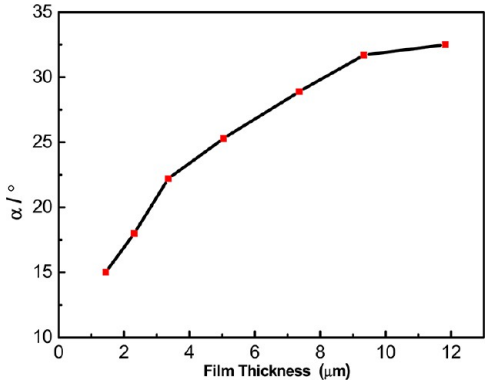

Figure 5. Characteristic wrinkling angle (α) of hierarchical wrinkles versus initial film thickness.

initial film thickness. The values of α were observed to increase from 14 to 33° as the initial thickness of the films increased from 1.4 to 11.8 μm. Theoretically, the angle is expected to approach 45° when the film is isotropically buckled at an infinite film thickness. However, as shown in Figure 4, at the film thickness is increased, the wrinkles start become more randomly-orientated. This indicates the confinement control of the imprinted nanoscale pattern diminishes with increasing underlying film thickness and films tend to be more isotropically compressed during the wrinkle development process. The size and depth of the imprinted lines remain constant while the underlying film thickness increases. Hence, the wrinkles become more randomly distributed and there would not be any observable characteristic wrinkle angle when the films become infinitely thick.

The wetting behavior of a surface depends largely on the degree and size scale of the surface roughness.[6,39] The roughness of the hierarchically wrinkled surface is determined by wrinkle size. The wavelength of the wrinkles was measured as the periodicity from a two-dimensional fast Fourier transform analysis of optical microscope images, while peak-to-valley (PV) distance and root mean square (RMS) roughness were determined by AFM analysis. Figure 6 presents the relationship between hierarchical wrinkle feature size and initial PHEMA film thickness. Wrinkle wavelength increases linearly with the film thickness at low film thickness region of 1.4−5.0 μm and the relationship between wrinkle wavelength and film thickness deviates from a single linear relation when the film thickness becomes larger. PV distance increases with increasing film thickness. The RMS roughness (R_q) can be defined as[40]

$$R_q = \sqrt{\frac{1}{L}\int_0^L z^2(x)dx} \tag{5}$$

where L is the evaluation length and $z(x)$ is the surface profile function. Herein, the surface profile is simplified to a sinusoidal surface as

$$z(x) = A\sin\left(\frac{2\pi}{\lambda}x\right) \tag{6}$$

where A is the amplitude of the sinusoidal wave and half of the PV distance, and λ is the wavelength. Substituting eq 6 into eq 5, we can obtain R_q as

$$R_q = A\sqrt{\frac{1}{\lambda}\int_0^\lambda \sin^2\left(\frac{2\pi}{\lambda}x\right)dx} \approx A \tag{7}$$

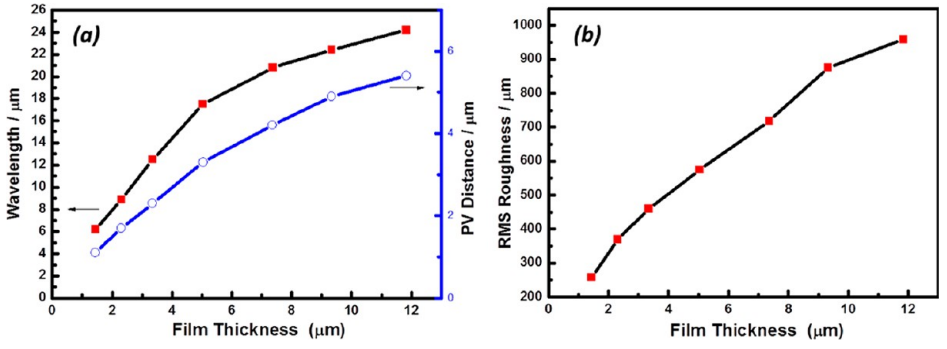

Figure 6. Relationship between hierarchical wrinkle feature size and film thickness: (a) wavelength and peak-to-valley (PV) distance, (b) root mean square roughness.

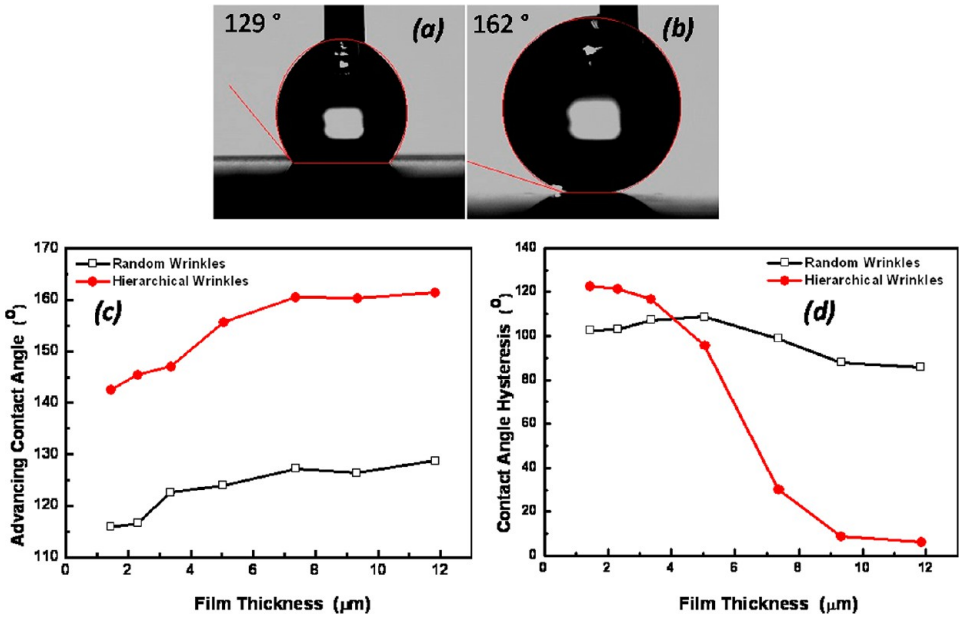

Figure 7. Optical images of a water droplet on the (a) random wrinkles and (b) hierarchical wrinkles. (c)Advancing contact angles and (d) contact angle hysteresis as a function of initial film thickness for random (open square symbol) and hierarchical wrinkles (close circle symbol).

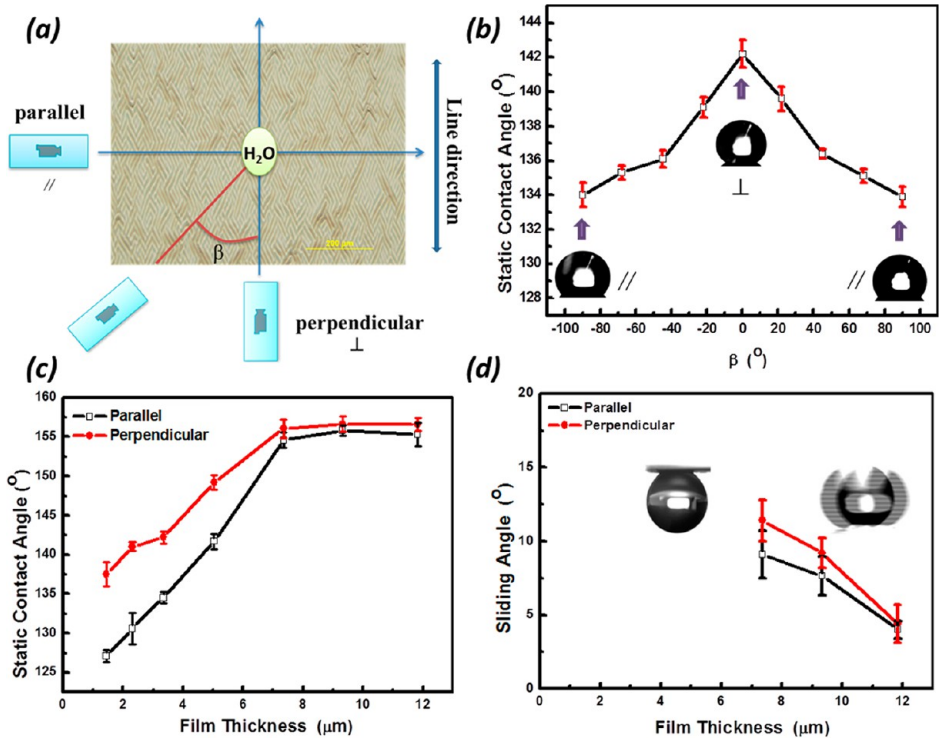

Figure 8. Anisotropic wetting behavior caused by pre-patterned grating nanostructures. (a) Schematic illustration of anisotropic wetting behavior; β is measuring angle relative to pre-imprinted line patterns, (b) static contact angles of hierarchical pattern with film thickness of 3.4 μm as a function of β (inset pictures are the optical images of water droplet at corresponding β), (c) static contact angles, and (d) sliding angles of both parallel (open square symbol) and perpendicular (close circle symbol) directions as a function of initial film thickness. Inset pictures in d are the optical images captured during sliding angle measurements.

Based on this simplified model, R_q is found to be proportional to amplitude. As a result of increasing wrinkle amplitude, the R_q of hierarchical wrinkle increases with film thickness (Figure 6b). Because our wrinkling system is similar to the work by Kim et al.,[24] who induced wrinkles by gradationally introducing silver nanoparticles into swollen polymer films, we attempted to apply their gradationally swollen model[24,41] to interpret the wrinkling behavior. However, the gradationally swollen model did not provide a reasonable explanation for the deviation from a single linear relation between wrinkle wavelength and film thickness and it does not provide a formula for the prediction of PV distances. Therefore, the gradationally swollen model as developed by Kim does not sufficiently clarify the wrinkling

dx.doi.org/10.1021/am403209r | ACS Appl. Mater. Interfaces 2013, 5, 11066−11073

phenomenon we observe. This presents opportunity for future investigation.

To investigate the wetting properties of our hierarchically wrinkled surfaces, dynamic water contact angle (CA) measurements were performed on films of various thickness. Panels a and b in Figure 7 show the optical images of water droplet on the random and hierarchical wrinkled PHEMA films with initial thickness of 11.8 μm. The random wrinkled surface was found to be hydrophobic with an average advancing CA value of 129° (Figure 7a). By comparison, the CAs of flat pure PHEMA film and methyltrichlorosilane treated silicon wafer (no shown) are 34 and 97°, respectively. The CA measurements results reveal that microscale roughness and surface chemical modification by silane infusion leads to an increase in hydrophobicity. More interestingly, the hierarchically wrinkled surfaces exhibited superhydrophobicity, in this case having contact angles greater than 160° (see Figure 7b). This indicates that the hierarchical nature of the roughness, i.e., the presence of micrometer-scale wrinkles containing a nanostructured grating pattern, significantly enhances the hydrophobicity of the surface.

Plots of the advancing CAs as a function of the film thickness for the random and hierarchical wrinkles are shown in Figure 7c, where CA values are observed to increase with increasing initial film thickness. In the case of the randomly wrinkled films, the advancing CA value increased from 115 to 128°. The hierarchically wrinkled surfaces with film thickness less than 5 μm showed a transition from hydrophobicity to superhydrophobicity with a linear increase of CA value from 142° to 150°. When the films had an initial thickness of >5 μm, the hierarchically wrinkled surfaces had advancing CAs greater than 150° and remained constant near 160° as the thickness increased beyond ~8 μm. Data from contact angle hysteresis (CAH) measurements—defined by the difference between advancing and receding contact angle of a drop of water—are shown in Figure 7d, where CAH of hierarchical wrinkles and random wrinkles has been plotted as a function of film thicknesses. The CAH of random wrinkles does not vary much with film thickness, whereas the CAH of hierarchically wrinkled surfaces was observed to change significantly. At low film thickness, the wetting state of the wrinkled surface is under the Wenzel state, the water droplet fully spans and wets the trench area of the line gratings, leading to higher pinning effect.[42] This pinning hinders the movement of the water contact line on the wrinkled surface leading to higher CAH than that of a comparable randomly wrinkled surface. As the film thickness is increased, the surface roughness increases as a result of increasing wrinkling PV distance. It is this higher surface roughness that enhances the hydrophobicity of wrinkled surface, leading to a transition of the wetting state from Wenzel state to the Cassie−Baxter state. Under the Cassie−Baxter wetting state, the water droplet does not wet the trench area of line gratings, which largely decreases the pinning effect of line gratings and accordingly the hysteresis decreases remarkably from more than 120° to less than 7°.

Because of the presence of the grating pattern, anisotropic wetting behavior of the hierarchical structures was expected.[43] Water CA measurements were taken at different angles (β) relative to the orientation of the grating lines as illustrated in Figure 8a. The CA of the perpendicular direction (β =0°) and parallel direction (β = ±90°) are defined as $\theta_\perp$ and $\theta_\parallel$, respectively. In Figure 8b, the CA of the 3.4 μm thick hierarchical patterned film is plotted as a function of measuring angle (β) relative to pre-imprinted line patterns. Here, the highest observed CA is $\theta_\perp$ =142°, while the lowest CA is $\theta_\parallel$ =134° and the degree of wetting anisotropy, $\Delta\theta$, is defined as the difference of the CA values from the two directions ($\Delta\theta = \theta_\parallel - \theta_\perp$= 8°). The change in CA is dependent on the value of β and the plot of CA is symmetric to β = 0° (perpendicular direction). This demonstrates that the anisotropic wetting behavior of the hierarchical patterns is related to the orientation of the line gratings. The effect of the wrinkle orientation was considered, but because the ratio of peak-to-valley (PV) distance to wrinkle wavelength (0.1−0.2) is much smaller than that of the aspect ratio of the line gratings (0.5), the wetting anisotropy can be primarily attributed to the pinning effect of line gratings rather than the wrinkles. Figure 8c shows that the static CA measured in both perpendicular and parallel directions increase with increasing film thickness (as well as wavelength and roughness of the surface topology), and reach at plateau of superhydrophobicity when the film thickness becomes greater than 7.4 μm. Similar anisotropic wetting behavior with $\Delta\theta \approx 7-10°$ was observed on the hierarchically wrinkled films with thickness ranging from 1.4 to 5.0 μm. A analogous anisotropic wettability due to pining effects of patterns was observed by Brennan et al. in their work on Sharklet patterns.[44] The origin of the wetting anisotropy was assigned to the pinning of the water droplet by the line patterns. The pinning effect imposes energy barriers which hinder the movement of the three-phase contact line in the perpendicular direction other than parallel direction, resulting in higher $\theta_\perp$ than $\theta_\parallel$. With increasing film thickness, both $\theta_\parallel$ and $\theta_\perp$ increase and reach a plateau value of about 157°. Meanwhile, as hierarchical surface roughness enhances the surface from hydrophobic to superhydrophobic, the anisotropy decreases to as low as 1°, implying a transition from anisotropic to isotropic wetting behavior. This remarkable wetting transition indicates that with increasing hydrophobicity, the contact area between the wrinkle surface and water droplet decreases to a very low extent that the water droplet does not wet the trench area of gratings and the pinning of grating patterns is greatly reduced, leading to isotropic wetting. These observed phenomena disclose a transition of the wetting state from the classic Wenzel state to the Cassie-Baxter state. The change of sliding angle (Figure 8d) confirms this transition as well. When the wetting is dictated by the Wenzel state, the water droplet wets the trench area of line pattern and the pinning effect prevents the sliding-off of water droplet from surface. Therefore, the droplet sticks to the wrinkled surface even if the substrate is turned upside down. On the contrary, once the wetting state turns to the Cassie state, the water droplet starts to slide at a very low tilt angle. With increasing hydrophobicity, the sliding angle decreases from around 10 to less than 5°. Because of the presence of line patterns, the sliding angle parallel to line patterns is slightly smaller than that perpendicular to the lines. Sliding angle and the difference of sliding angle between two directions diminish with increasing film thickness. Chung et al.[45] observed anisotropic wetting behavior as a function of wrinkling amplitude in their wrinkling system. Unlike our work, they did not observe the anisotropic to isotropic wettability transition with increasing wrinkling size. Conversely, they presented an enhanced anisotropic wettability as $\theta_\perp$ increased, whereas $\theta_\parallel$ decreased with increasing surface roughness. This difference is attributed to the roughness-enhanced wetting. Because there is no motion barrier caused pinning effect for liquid to move parallel to the grooves,

roughness-enhanced wetting dominate the change of $\theta_{\parallel}$. According to Wenzel equation[46]

$$\cos\theta = r\cos\theta_0 \quad (8)$$

where r is the roughness factor and θ_0 is the contact angle of flat surface. The UVO-modified PDMS surface is initially hydrophilic, accordingly the increment of surface roughness would give rise to the decrease of $\theta_{\parallel}$ in their work. The increase of $\theta_{\perp}$ is due to groove pinning and the decrease of $\theta_{\parallel}$ is caused by roughness-enhanced wetting which contributes to the enhanced anisotropic wettability. In contrast, our system contains a methyltrichlorosilane-modified surface which is much more hydrophobic in nature than an oxidized silicone elastomer, therefore, both $\theta_{\perp}$ and $\theta_{\parallel}$ increase with increasing surface roughness, resulting in a transition from anisotropic to isotropic wetting behavior.

CONCLUSIONS

We report a new method for creating hierarchically wrinkled polymer films by combining top-down nanoimprint lithography and a bottom-up wrinkling process. The resulting hierarchical wrinkle patterns exhibit regularly ordered herringbone structures accomplished through the geometric confinement of the imprinted nanopatterns. Further, these surfaces are superhydrophobic with water contact angles higher than 160°. This behavior is due to the complementary micro/nano dual scale roughness presented by the surface. The wettability of the surfaces can be controlled by altering the film thickness giving excellent control from hydrophobic to superhydrophobic as well as an extraordinary transition from anisotropic to isotropic wetting. This work provides a controlled simple, efficient method to prepare superhydrophobic surfaces which will present opportunities for exploitation in a number of known potential applications, such as self-cleaning, antibacterial surfaces and drag reduction. The anisotropic surfaces offer hierarchical roughness, which might also be beneficial for applications in adhesion, artificial skin, gas sensors, light sensors, etc. The nature of the three-step process, coating, imprinting followed by chemical infusion, makes it easy to implement over large areas and does not require complex processing equipment or time-consuming preparation which makes these surfaces amenable to high-throughput manufacturing methods such as roll-to-roll fabrication.

AUTHOR INFORMATION

Corresponding Author

*E-mail: krcarter@polysci.umass.edu. Phone: +001-413-577-1416. Fax: +001-413-545-0082.

Notes

The authors declare no competing financial interest.

ACKNOWLEDGMENTS

This research was kindly supported by the NSF Material Research Science and Engineering Center on Polymers at UMass (MRSEC) (DMR-0213695), the UMass Center for Hierarchical Manufacturing (CHM), a NSF Nanoscale Science and Engineering Center (CMMI-1025020), as well as a kind grant from the Panasonic Boston Laboratory. Dai also thanks the National Natural Science Foundation of China (20903034) for support.

REFERENCES

(1) Zhang, X.; Shi, F.; Niu, J.; Jiang, Y. G.; Wang, Z. Q. *J. Mater. Chem.* **2008**, *18*, 621−633.
(2) Li, X. M.; Reinhoudt, D.; Crego-Calama, M. *Chem. Soc. Rev.* **2007**, *36*, 1529−1529.
(3) Bhushan, B.; Jung, Y. C.; Koch, K. *Philos. Trans. R. Soc. London, Ser. A* **2009**, *367*, 1631−1672.
(4) Efimenko, K.; Finlay, J.; Callow, M. E.; Callow, J. A.; Genzer, J. *ACS Appl. Mater. Interfaces* **2009**, *1*, 1031−1040.
(5) Feng, X. J.; Jiang, L. *Adv. Mater.* **2006**, *18*, 3063−3078.
(6) Lee, S. G.; Lim, H. S.; Lee, D. Y.; Kwak, D.; Cho, K. *Adv. Funct. Mater.* **2013**, *23*, 547−553.
(7) Xue, C. H.; Jia, S. T.; Zhang, J.; Ma, J. Z. *Sci. Technol. Adv. Mater.* **2010**, *11*, 3002.
(8) Ou, J. F.; Hu, W. H.; Xue, M. S.; Wang, F. J.; Li, W. *ACS Appl. Mater. Interfaces* **2013**, *5*, 3101−3107.
(9) Guo, L. J. *Adv. Mater.* **2007**, *19*, 495−513.
(10) Lan, H.; Ding, Y.; Liu, H.; Lu, B. *Microelectron. Eng.* **2007**, *84*, 684−688.
(11) Zhang, F. X.; Low, H. Y. *Langmuir* **2007**, *23*, 7793−7798.
(12) Liu, X. J.; Wu, W. C.; Wang, X. L.; Luo, Z. Z.; Liang, Y. M.; Zhou, F. *Soft Matter* **2009**, *5*, 3097−3105.
(13) Chang, K. C.; Lu, H. I.; Peng, C. W.; Lai, M. C.; Hsu, S. C.; Hsu, M. H.; Tsai, Y. K.; Chang, C. H.; Hung, W. I.; Wei, Y.; Yeh, J. M. *ACS Appl. Mater. Interfaces* **2013**, *5*, 1460−1467.
(14) Liu, B.; He, Y. N.; Fan, Y.; Wang, X. G. *Macromol. Rapid Commun.* **2006**, *27*, 1859−1864.
(15) Saison, T.; Peroz, C.; Chauveau, V.; Berthier, S.; Sondergard, E.; Arribart, H. *Bioinspiration Biomimetics* **2008**, *3*, 046004.
(16) Jeong, H. E.; Kwak, R.; Khademhosseini, A.; Suh, K. Y. *Nanoscale* **2009**, *1*, 331−338.
(17) Yang, S.; Khare, K.; Lin, P. C. *Adv. Funct. Mater.* **2010**, *20*, 2550−2564.
(18) Li, B.; Cao, Y. P.; Feng, X. Q.; Gao, H. J. *Soft Matter* **2012**, *8*, 5728−5745.
(19) Huntington, M. D.; Engel, C. J.; Hryn, A. J.; Odom, T. W. *ACS Appl. Mater. Interfaces* **2013**, *5*, 6438−6442.
(20) Zhang, Z. Q.; Zhang, T.; Zhang, Y. W.; Kim, K. S.; Gao, H. J. *Langmuir* **2012**, *28*, 2753−2760.
(21) Rahmawan, Y.; Moon, M. W.; Kim, K. S.; Lee, K. R.; Suh, K. Y. *Langmuir* **2010**, *26*, 484−491.
(22) Lee, S. G.; Lee, D. Y.; Lim, H. S.; Lee, D. H.; Lee, S.; Cho, K. *Adv. Mater.* **2010**, *22*, 5013−5017.
(23) Lin, P. C.; Yang, S. *Soft Matter* **2009**, *5*, 1011−1018.
(24) Kim, Y. H.; Lee, Y. M.; Lee, J. Y.; Ko, M. J.; Yoo, P. J. *ACS Nano* **2012**, *6*, 1082−1093.
(25) Li, Y.; Peterson, J. J.; Jhaveri, S. B.; Carter, K. R. *Langmuir* **2013**, *29*, 4632−4639.
(26) Erenturk, B.; Gurbuz, S.; Corbett, R. E.; Claiborne, S.-A. M.; Krizan, J.; Venkataraman, D.; Carter, K. R. *Chem. Mater.* **2011**, *23*, 3371−3376.
(27) Park, J.-Y.; Chae, H. Y.; Chung, C.-H.; Sim, S. J.; Park, J.; Lee, H. H.; Yoo, P. J. *Soft Matter* **2010**, *6*, 677−684.
(28) Guo, C. F.; Nayyar, V.; Zhang, Z.; Chen, Y.; Miao, J.; Huang, R.; Liu, Q. *Adv. Mater.* **2012**, *24*, 3010−3014.
(29) Lee, J. H.; Ro, H. W.; Huang, R.; Lemaillet, P.; Germer, T. A.; Soles, C. L.; Stafford, C. M. *Nano Lett.* **2012**, *12*, 5995−5999.
(30) Khang, D. Y.; Jiang, H. Q.; Huang, Y.; Rogers, J. A. *Science* **2006**, *311*, 208−212.
(31) Ding, W. L.; Yang, Y.; Zhao, Y.; Jiang, S. C.; Cao, Y. P.; Lu, C. H. *Soft Matter* **2013**, *9*, 3720−3726.
(32) Breid, D.; Crosby, A. J. *Soft Matter* **2009**, *5*, 425−431.
(33) Chan, E. P.; Crosby, A. J. *Soft Matter* **2006**, *2*, 324−328.
(34) Bowden, N.; Brittain, S.; Evans, A. G.; Hutchinson, J. W.; Whitesides, G. M. *Nature* **1998**, *393*, 146−149.
(35) Genzer, J.; Groenewold, J. *Soft Matter* **2006**, *2*, 310−323.
(36) Ohzono, T.; Matsushita, S. I.; Shimomura, M. *Soft Matter* **2005**, *1*, 227−230.
(37) Lin, P. C.; Yang, S. *Appl. Phys. Lett.* **2007**, *90*, 241903−241903.

(38) Yin, J.; Yague, J. L.; Eggenspieler, D.; Gleason, K. K.; Boyce, M. C. *Adv. Mater.* **2012**, *24*, 5441−5446.
(39) Nosonovsky, M.; Bhushan, B. *Microelectron. Eng.* **2007**, *84*, 382−386.
(40) Thomas, T. R. *Rough Surfaces*, 2nd ed.; Imperial College Press: London, 1999; p 137.
(41) Tanaka, T.; Sun, S. T.; Hirokawa, Y.; Katayama, S.; Kucera, J.; Hirose, Y.; Amiya, T. *Nature* **1987**, *325*, 796−798.
(42) Sommers, A. D.; Jacobi, A. M. *J. Micromech. Microeng.* **2006**, *16*, 1571−1578.
(43) Xia, D.; Johnson, L. M.; Lopez, G. P. *Adv. Mater.* **2012**, *24*, 1287−302.
(44) Long, C. J.; Schumacher, J. F.; Brennan, A. B. *Langmuir* **2009**, *25*, 12982−12989.
(45) Chung, J. Y.; Youngblood, J. P.; Stafford, C. M. *Soft Matter* **2007**, *3*, 1163−1169.
(46) Wenzel, R. N. *Ind. Eng. Chem.* **1936**, *28*, 988−994.